

# Revisiting Invariant Learning for Out-of-Domain Generalization on Multi-Site Mammogram Datasets

Hung Q. Vo, Samira Zare, Son T. Ly, Lin Wang, Chika F. Ezeana, Xiaohui Yu,  
Kelvin K. Wong, Stephen T.C. Wong\*, and Hien V. Nguyen\*

**Abstract**—Despite significant progress in robust deep learning techniques for mammogram breast cancer classification, their reliability in real-world clinical development settings remains uncertain. The translation of these models to clinical practice faces challenges due to variations in medical centers, imaging protocols, and patient populations. To enhance their robustness, invariant learning methods have been proposed, prioritizing causal factors over misleading features. However, their effectiveness in clinical development and impact on mammogram classification require investigation. This paper reassesses the application of invariant learning for breast cancer risk estimation based on mammograms. Utilizing diverse multi-site public datasets, it represents the first study in this area. The objective is to evaluate invariant learning’s benefits in developing robust models. Invariant learning methods, including Invariant Risk Minimization and Variance Risk Extrapolation, are compared quantitatively against Empirical Risk Minimization. Evaluation metrics include accuracy, average precision, and area under the curve. Additionally, interpretability is examined through class activation maps and visualization of learned representations. This research examines the advantages, limitations, and challenges of invariant learning for mammogram classification, guiding future studies to develop generalized methods for breast cancer prediction on whole mammograms in out-of-domain scenarios.

**Index Terms**—component, formatting, style, styling, insert

## I. INTRODUCTION

While numerous studies have investigated how robust deep learning is for breast cancer risk prediction based on mammograms [1]–[3], there are still lingering concerns about the reliability and generalizability of these algorithms. In a recent study by Barros et al. [4], they conducted a preliminary investigation into the generalizability of their CNN image model across two continents, Israel and the United States. Their approach involved training the models on data from one continent and evaluating their performance on data from the other continent. As anticipated, the authors observed a decline in performance when applying the models to out-of-domain data, which they attributed to variations in health policies and demographic populations between the two continents. However, the study did not delve into the exploration of recent domain generalization methods that could enhance the models’ adaptability to out-of-domain distributions. Additionally, the

study was limited by its inclusion of data from only two continents, namely the USA and Israel. In our paper, we aim to overcome these limitations by conducting a comprehensive investigation into the generalization of mammogram deep models using a substantial number of multi-site datasets.

In another study by De et al. [5], the researchers explore the generalizability of an AI commercial tool to an external dataset generated using different mammography equipment. They investigate whether the performance of the AI commercial tool can be maintained when applied to data acquired from varied equipment sources. The paper suggests that calibration of the AI decision threshold could potentially mitigate the impact of mammography equipment software upgrades on the tool’s recall rate. However, the study acknowledges that the implementation of AI in clinical practice necessitates local retrospective evaluation and ongoing quality assurance measures. A limitation of the study is its focus on a single-site setting and a predominantly White Caucasian sample population. In contrast, our paper addresses this limitation by conducting experiments on a large number of public mammogram datasets obtained from diverse continents, thereby enhancing the generalizability and inclusivity of our findings.

Invariant risk minimization [6], [7] is a machine learning algorithm that focuses on developing models capable of robustly generalizing across various environments or domains. The fundamental principle of IRM involves explicitly optimizing for invariance to specific factors or variables that may exhibit variations across different domains. Leveraging this framework can be particularly beneficial when working with medical imaging data sourced from diverse hospitals or institutions spanning across continents [8].

Although a previous study has employed invariant learning for mammogram classification [9], its focus is primarily on analyzing lesion crops extracted from mammograms. Additionally, it is limited in terms of evaluation as it primarily utilizes private datasets, with only one public dataset, CBIS-DDSM, being employed. As far as we know, our research is the first to investigate domain-invariant learning for classifying whole mammograms. Furthermore, all the datasets utilized in this paper are available online. We aim for this study to establish a foundation for future research on developing generalized approaches on whole mammograms for the prediction of breast cancer in challenging out-of-domain scenarios.

Identify applicable funding agency here. If none, delete this.

\* Hien V. Nguyen and Stephen T.C. Wong are co-senior authors

Hung Q. Vo, Samira Zare, Son T. Ly, and Hien V. Nguyen are with the Department of Electrical and Computer Engineering, University of Houston, Houston, TX 77204 USA.

Lin Wang, Chika F. Ezeana, Xiaohui Yu, Kelvin K. Wong, and Stephen T.C. Wong are with Department of Systems Medicine and Biomedical Engineering, Houston Methodist Cancer Center, Houston, TX 77030 USA.

## II. METHODS

### A. Mammograms classification with tiled patches classifier initialization using CNNs

In the domain of whole mammogram classification, we build upon prior research that has demonstrated the effectiveness of CNNs [10]–[12]. In line with the approach presented in [10], our methodology involves initial training of the network using tiled patches, encompassing both lesion patches and background crops. Subsequently, the pre-trained network serves as the starting point for initializing the whole mammogram network. In this study, we employ a standard residual network (ResNet) [13], and a more modernized ConvNet (ConvNeXt) [14], which has demonstrated competitive accuracy and scalability compared to the Vision Transformer [15].

### B. Invariant Learning algorithms

1) *Invariant Risk Minimization (IRM)*: Invariant Risk Minimization (IRM) [6] is a learning approach that focuses on estimating consistent correlations across diverse training distributions. By learning a data representation that ensures an optimal classifier performs well across all training distributions, IRM enables effective generalization to out-of-distribution scenarios. This capability is particularly valuable in real-world applications such as medical diagnosis, where the data distribution can vary significantly across different hospitals and institutions. The invariances captured by IRM are associated with the underlying causal structures that govern the data, enhancing its ability to uncover meaningful patterns and relationships.

Let  $e \in \mathcal{E}$  be an environment with its own data distribution  $\mathcal{X}, \mathcal{Y}$ . Denote  $\mathcal{E}_{\text{tr}} \subset \mathcal{E}$ ,  $\mathcal{E}_{\text{tr}}$  is an empirical set of environments or a set of environments that can be accessed. Let  $\Phi : \mathcal{X} \rightarrow \mathcal{H}$  be a projection function of data into the latent space.  $R^e(\Phi)$  will be a risk of environment  $e$  under  $\Phi$ . The practical IRM objective is:

$$\Phi^* = \arg \min_{\Phi: \mathcal{X} \rightarrow \mathbb{R}^d} \sum_{e \in \mathcal{E}_{\text{tr}}} R^e(\Phi) + \lambda (\nabla_w R^e(w \cdot \Phi)|_{w=1})^2 \quad (1)$$

Here,  $w$  is a simplified version of the predictor  $g : \mathcal{H} \rightarrow \mathcal{Y}$  which is assumed to be optimal over all environments. To streamline the learning process, the value of  $w$  is fixed at 1, allowing the network to concentrate on learning the representations captured by  $\Phi$ .

2) *Variance Risk Extrapolation (VREx)*: Risk Extrapolation (REx) [7] demonstrates superior performance compared to Invariant Risk Minimization (IRM) when faced with scenarios where both causally induced distributional shifts and covariate shifts occur simultaneously. REx achieves this by effectively balancing its resilience to these types of shifts. In contrast, IRM assumes that the learned invariances from the training data alone are adequate for generalization to new domains, which may not always hold true. While both REx and IRM are capable of performing causal identification, REx demonstrates greater robustness in handling covariate shifts (changes in the input distribution). Covariate shift poses challenges when

models are misspecified, when training data is limited, or when it fails to cover relevant areas of the test distribution.

REx is a robust optimization technique that operates within a perturbation set of extrapolated domains. Another variant, named VREx, introduces a penalty term that targets the variance of training risks. It has been shown that variants of REx can recover the causal mechanisms of the targets, while also providing some robustness to changes in the input distribution. VREx shares a similar objective to IRM but replaces the penalty term with the variance of training risks across different environments:

$$\Phi^* = \arg \min_{\Phi: \mathcal{X} \rightarrow \mathbb{R}^d} [\lambda \text{Var}(\{R^e(\Phi)\}_{e \in \mathcal{E}_{\text{tr}}}) + \sum_{e \in \mathcal{E}_{\text{tr}}} R^e(\Phi)] \quad (2)$$

3) *Invariant Learning on multi-site datasets*: In our study, we adopt the perspective that each dataset obtained from a particular hospital or institution represents a distinct environment. The training process involves straightforward computation of risks for each dataset, followed by the calculation of either the IRM or VREx objective. To ensure the validity of our approach, we ensure that the datasets used for training and testing originate from different sites or institutions. This approach enables us to evaluate the performance of our models across diverse environments and establish their robustness in handling variations between different data sources [17].

## III. EXPERIMENTS

### A. Datasets

All the datasets utilized in this research are readily available online, ensuring accessibility for future studies and enabling fair comparisons. The datasets employed in this paper include: CBIS-DDSM (USA) [18], EMBED (USA) [19], INbreast (Portugal) [20], BMCD (Republic of Cyprus) [21], BCDR (Portuguese) [22], CDD-CESM (Egypt) [23], and CSAW-CC (Sweden) [24].

For conducting out-of-domain experiments, we utilize CDD-CESM and CSAW-CC datasets for testing, which originate from countries not represented in the training set. The remaining datasets are employed for training purposes. As for in-domain experiments, the official test set of CBIS-DDSM and 25% of the EMBED dataset are utilized. Special care is taken to ensure that there are no overlapping patients between the train and test splits during the dataset partitioning process.

### B. Experiment Settings

Table I displays the results of all experiments conducted. We employ two network architectures, namely ResNet34 and ConvNeXt-tiny, focusing solely on CNNs for our study. ConvNeXt has exhibited competitive accuracy and scalability compared to vision transformer [14], making it a compelling choice for our research. Our training approach involves training on smaller images initially (lesion patches, background crops) and subsequently retraining on larger images (whole mammograms). This sequential training strategy has been proven effective in improving whole-mammogram classification, as demonstrated by Shen et al. [10].

Model	Method	CBIS-DDSM test (in-domain)			EMBED test (in-domain)			CDD-CESM (ood)			CSAWCC (ood)		
		Acc	AP	AUROC	Acc	AP	AUROC	Acc	AP	AUROC	Acc	AP	AUROC
ResNet34	ERM [16]	0.648	0.729	0.785	0.703	0.437	0.524	0.733	<b>0.651</b>	<b>0.740</b>	0.984	<b>0.081</b>	<b>0.664</b>
	ERM*	0.566	<b>0.745</b>	0.788	0.738	<b>0.559</b>	0.630	0.692	0.508	0.652	0.979	0.032	0.549
	IRM [6]	0.602	0.388	0.460	0.609	0.266	0.391	0.673	0.289	0.436	0.990	0.010	0.495
	VREx [7]	0.570	0.741	<b>0.797</b>	0.641	0.521	<b>0.641</b>	0.644	0.545	0.672	0.914	0.059	0.628
ConvNeXt-tiny	ERM [16]	0.733	<b>0.742</b>	<b>0.797</b>	0.814	<b>0.719</b>	0.746	0.794	<b>0.731</b>	<b>0.832</b>	0.979	<b>0.108</b>	<b>0.727</b>
	ERM*	0.712	0.719	0.759	0.795	0.676	0.705	0.759	0.697	0.798	0.980	0.070	0.669
	IRM [6]	0.401	0.527	0.590	0.326	0.513	0.604	0.618	0.577	0.709	0.989	0.019	0.580
	VREx [7]	0.638	0.731	0.775	0.762	0.671	<b>0.748</b>	0.729	0.679	0.785	0.953	0.064	0.596

TABLE I

EVALUATION RESULTS FOR WHOLE-MAMMOGRAM CANCER CLASSIFICATION. ALL EXPERIMENTS WERE CONDUCTED USING MAMMOGRAMS WITH A RESOLUTION OF 576X448 PIXELS. (\*: APPROXIMATED BY IGNORING PENALIZATION TERM IN IRM)

To initiate the training of whole-mammogram experiments, we pre-train a single patch classifier. Following the strategy by Shen et al. [10], we use augmented crops of lesion and background patches. The training data for the patch classifier includes CBIS-DDSM [18], EMBED [19], INbreast [20], and BCDR [22] datasets, all of which provide ground-truth annotations for lesions.

All whole-mammogram classifiers undergo evaluation using four distinct datasets that were not included in the training phase. For in-domain evaluation, we utilize the official test set of CBIS-DDSM and a subset comprising 25% of the EMBED dataset. Although these datasets contain the same type of mammograms, they were not used during the model’s training. To assess out-of-domain generalization, we employ the CDD-CESM and CSAWCC datasets. The mammograms from these two datasets were not encountered by the model during the training process.

All experiments in our study are trained using the Adam optimizer with a learning rate of  $1e-3$ . Due to computational limitations, mammograms are resized to a resolution of 576x448. While higher resolutions have demonstrated performance improvements, such as 1152x896 [10] or even larger [25], we have chosen to focus on smaller resolutions to accommodate our available computational resources.

### C. Quantitative Results

Table I shows evaluation results for in-domain and out-of-domain experiments. For each model architecture, four learning algorithms, ERM [16], approximated ERM (by setting penalization term to zero in IRM [6]), IRM [6], and VREx [7] are evaluated.

In the case of the two in-domain datasets, both ERM and VREx demonstrate the highest performance. When using VREx, ResNet34 achieves an AUC of 0.797 on the CBIS-DDSM test set and an AUC of 0.641 on the EMBED test set. For ConvNeXt-tiny, ERM achieves the highest results in terms of both average precision (AP) and AUC. VREx follows closely behind with a slightly higher AUC on the EMBED test set. Notably, ConvNeXt consistently outperforms ResNet34 with a significant performance gap observed on the EMBED test set, highlighting the effectiveness of this modernized CNN architecture on mammogram data. IRM consistently exhibits the lowest performance across both in-domain and out-of-

domain datasets. A careful analysis of the training metrics reveals a significant decline in performance after applying IRM, suggesting a potential issue of underfitting. We suspect that more appropriate hyperparameters for IRM are required to achieve better results. However, this observation underscores the unstable training behavior of IRM in our experiments.

For out-of-domain evaluations, we utilize CDD-CESM and CSAWCC datasets, which originate from institutions and nationalities distinct from the training datasets. Among the methods evaluated, ERM demonstrates the highest performance, closely followed by approximated ERM and VREx. Notably, ConvNeXt-tiny consistently outperforms ResNet34, achieving the highest AUC scores on both datasets when using ERM (0.832 on CDD-CESM and 0.727 on CSAWCC). This indicates that, in terms of evaluation metrics, normal training yields higher scores than invariant learning in our experiments. However, to gain further insights into the prediction process of these methods, we will proceed to visualize the learned features of the two top-performing methods: ERM and VREx. This qualitative evaluation aims to explore the differences between normal learning and invariant learning.

### D. Qualitative Results

We generate Class Activation Maps (CAM) to visualize the activation patterns of the top-performing methods, ERM and VREx. In Figure 1 and Figure 2, we present the CAMs for ResNet34d, showcasing both successful and unsuccessful results. Similarly, Figure 3 and Figure 4 depict the CAMs for ConvNeXt, highlighting instances of good and failed predictions. These visualizations provide insights into the discriminative regions of the images that contribute to the model’s decision-making process.

In the first two rows of Figure 1, both ERM and VREx consistently focus on the correct regions of interest. However, in some cases, ERM deviates and attends to other areas of the breast (rows 3 and 4) or even background regions (rows 5 and 6). Similar observations can be made for ConvNeXt, where ERM and VREx primarily concentrate on the appropriate regions (rows 1, 2, and 3). However, there are instances where ERM directs attention to different breast regions (rows 5 and 6) or background areas (row 4).

In the failed results, both ResNet34d and ConvNeXt-tiny exhibit similar errors. In some cases, both methods attend to

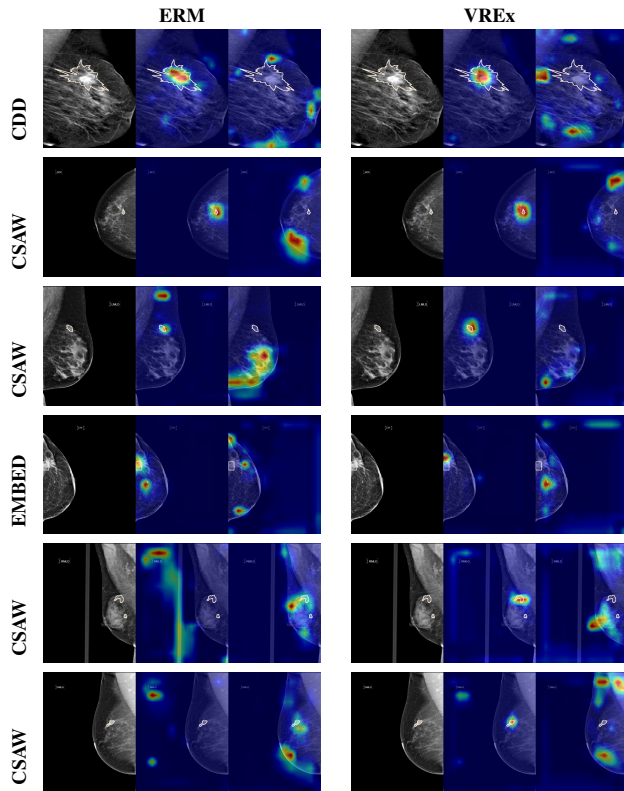


Fig. 1. Activation maps with good results - ResNet34d (Column headers describe the used method. Row texts are for the dataset name. For each subfigure, we show three images: original mammogram, activation map for malignant cases, and activation map for benign cases)

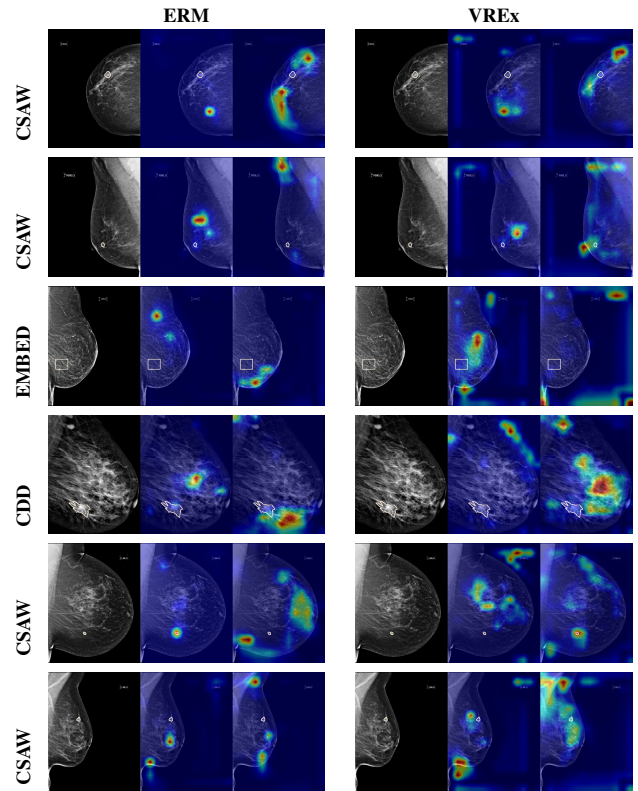


Fig. 2. Activation maps with failed results - ResNet34d (Column headers describe the used method. Row texts are for the dataset name. For each subfigure, we show three images: original mammogram, activation map for malignant cases, and activation map for benign cases)

the same incorrect regions (rows 1 and 2 in Figure 2 or rows 1 and 2 in Figure 4). In other instances, they fail in different ways, with each method focusing on different incorrect cues (rows 3 to 6 in Figure 2 and Figure 4). These findings suggest that, in some cases, both methods encounter challenges in accurately identifying the correct regions of interest.

#### IV. CONCLUSION

In this research paper, we conducted experiments focusing on domain invariant learning specifically for whole-mammogram data. Our study utilized a substantial amount of publicly available mammogram datasets for both training and evaluation purposes. Two methods, namely Invariant Risk Minimization (IRM) and Variance Risk Extrapolation (VREx), were employed in our investigation. While we observed unstable training patterns in IRM for mammogram classification, VREx displayed promising results. However, Empirical Risk Minimization (ERM) still achieved the best numerical performance. Our findings highlight the need to explore more domain-invariant techniques and to guide future studies to develop generalized methods for breast cancer prediction on whole mammograms in out-of-domain scenarios.

#### REFERENCES

[1] A. Yala, P. G. Mikhael, F. Strand, G. Lin, K. Smith, Y.-L. Wan, L. Lamb, K. Hughes, C. Lehman, and R. Barzilay, "Toward robust mammography-

based models for breast cancer risk," *Science Translational Medicine*, vol. 13, no. 578, p. eaba4373, 2021.

[2] A. Yala, P. G. Mikhael, F. Strand, G. Lin, S. Satuluru, T. Kim, I. Banerjee, J. Gichoya, H. Trivedi, C. D. Lehman *et al.*, "Multi-institutional validation of a mammography-based breast cancer risk model," *Journal of Clinical Oncology*, vol. 40, no. 16, pp. 1732–1740, 2022.

[3] W. Lotter, A. R. Diab, B. Haslam, J. G. Kim, G. Grisot, E. Wu, K. Wu, J. O. Onieva, Y. Boyer, J. L. Boxerman *et al.*, "Robust breast cancer detection in mammography and digital breast tomosynthesis using an annotation-efficient deep learning approach," *Nature Medicine*, vol. 27, no. 2, pp. 244–249, 2021.

[4] V. Barros, T. Tlustý, E. Barkan, E. Hexter, D. Gruen, M. Guindy, and M. Rosen-Zvi, "Virtual biopsy by using artificial intelligence-based multimodal modeling of binational mammography data," *Radiology*, p. 220027, 2022.

[5] C. F. de Vries, S. J. Colosimo, R. T. Staff, J. A. Dymiter, J. Yearsley, D. Dinneen, M. Boyle, D. J. Harrison, L. A. Anderson, G. Lip *et al.*, "Impact of different mammography systems on artificial intelligence performance in breast cancer screening," *Radiology: Artificial Intelligence*, vol. 5, no. 3, p. e220146, 2023.

[6] M. Arjovsky, L. Bottou, I. Gulrajani, and D. Lopez-Paz, "Invariant risk minimization," *arXiv preprint arXiv:1907.02893*, 2019.

[7] D. Krueger, E. Caballero, J.-H. Jacobsen, A. Zhang, J. Binas, D. Zhang, R. Le Priol, and A. Courville, "Out-of-distribution generalization via risk extrapolation (rex)," in *International Conference on Machine Learning*. PMLR, 2021, pp. 5815–5826.

[8] D. C. Castro, I. Walker, and B. Glocker, "Causality matters in medical imaging," *Nature Communications*, vol. 11, no. 1, p. 3673, 2020.

[9] C. Wang, J. Li, X. Sun, F. Zhang, Y. Yu, and Y. Wang, "Domain invariant model with graph convolutional network for mammogram classification," *arXiv preprint arXiv:2204.09954*, 2022.

[10] L. Shen *et al.*, "Deep learning to improve breast cancer detection on screening mammography," *Scientific reports*, vol. 9, no. 1, pp. 1–12, 2019.

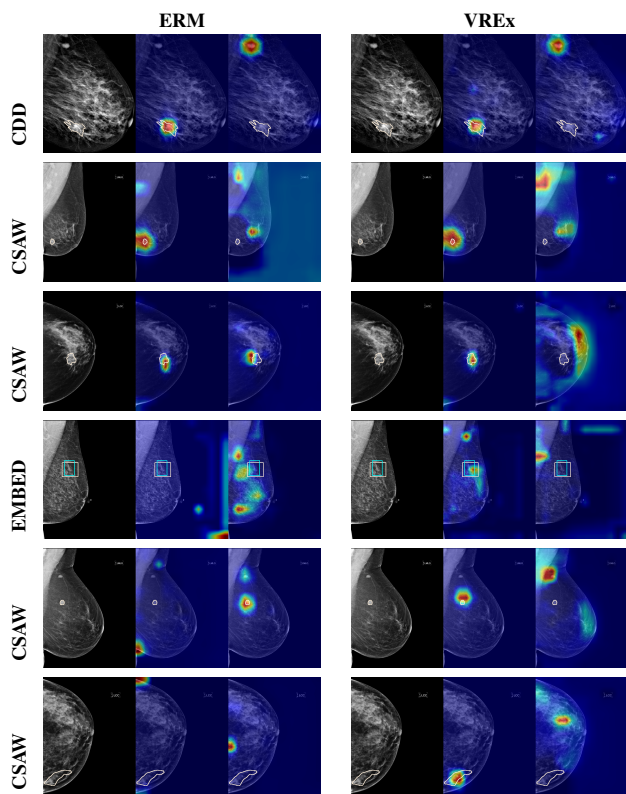


Fig. 3. Activation maps with good results - ConvNeXt-tiny (Column headers describe the used method. Row texts are for the dataset name. For each subfigure, we show three images: original mammogram, activation map for malignant cases, and activation map for benign cases)

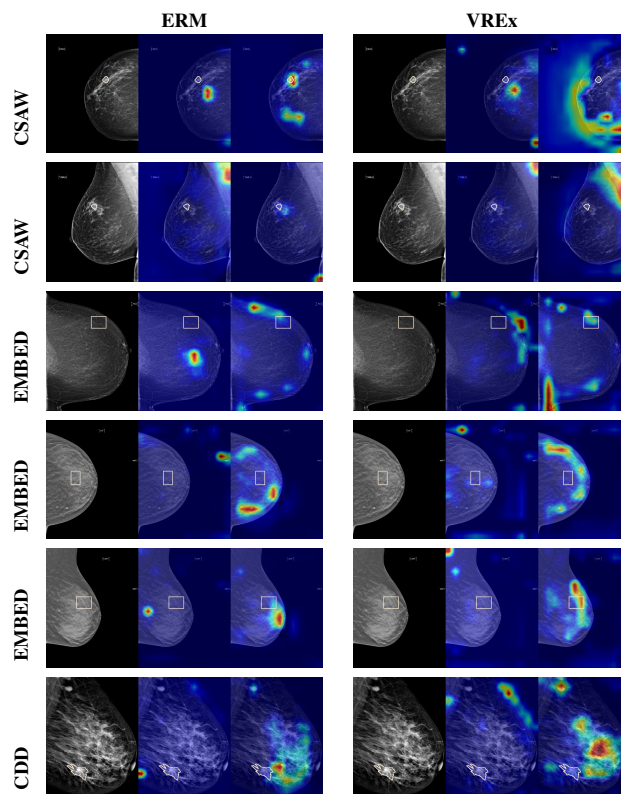


Fig. 4. Activation maps with failed results - ConvNeXt-tiny (Column headers describe the used method. Row texts are for the dataset name. For each subfigure, we show three images: original mammogram, activation map for malignant cases, and activation map for benign cases)

- [11] I. Sechopoulos, J. Teuwen, and R. Mann, "Artificial intelligence for breast cancer detection in mammography and digital breast tomosynthesis: State of the art," in *Seminars in Cancer Biology*, vol. 72. Elsevier, 2021, pp. 214–225.
- [12] N. Sharma, A. Y. Ng, J. J. James, G. Khara, E. Ambrozay, C. C. Austin, G. Forrai, G. Fox, B. Glocker, A. Heindl *et al.*, "Retrospective large-scale evaluation of an ai system as an independent reader for double reading in breast cancer screening," *medRxiv*, pp. 2021–02, 2021.
- [13] K. He, X. Zhang, S. Ren, and J. Sun, "Deep residual learning for image recognition," in *Proceedings of the IEEE conference on computer vision and pattern recognition*, 2016, pp. 770–778.
- [14] Z. Liu, H. Mao, C.-Y. Wu, C. Feichtenhofer, T. Darrell, and S. Xie, "A convnet for the 2020s," in *Proceedings of the IEEE/CVF Conference on Computer Vision and Pattern Recognition*, 2022, pp. 11 976–11 986.
- [15] A. Dosovitskiy, L. Beyer, A. Kolesnikov, D. Weissenborn, X. Zhai, T. Unterthiner, M. Dehghani, M. Minderer, G. Heigold, S. Gelly *et al.*, "An image is worth 16x16 words: Transformers for image recognition at scale," *arXiv preprint arXiv:2010.11929*, 2020.
- [16] V. Vapnik, "Principles of risk minimization for learning theory," *Advances in neural information processing systems*, vol. 4, 1991.
- [17] I. Gulrajani and D. Lopez-Paz, "In search of lost domain generalization," *arXiv preprint arXiv:2007.01434*, 2020.
- [18] R. S. Lee *et al.*, "A curated mammography data set for use in computer-aided detection and diagnosis research," *Scientific data*, vol. 4, no. 1, pp. 1–9, 2017.
- [19] J. J. Jeong, B. L. Vey, A. Bhimoreddy, T. Kim, T. Santos, R. Correa, R. Dutt, M. Mosunjac, G. Oprea-Ilieș, G. Smith *et al.*, "The emory breast imaging dataset (embed): A racially diverse, granular dataset of 3.4 million screening and diagnostic mammographic images," *Radiology: Artificial Intelligence*, vol. 5, no. 1, p. e220047, 2023.
- [20] I. C. Moreira *et al.*, "Inbreast: toward a full-field digital mammographic database," *Academic radiology*, vol. 19, no. 2, pp. 236–248, 2012.
- [21] K. Loizidou, G. Skouroumouni, C. Pitris, and C. Nikolaou, "Digital subtraction of temporally sequential mammograms for improved detection and classification of microcalcifications," *European radiology experimental*, vol. 5, no. 1, pp. 1–12, 2021.
- [22] D. C. Moura *et al.*, "Benchmarking datasets for breast cancer computer-aided diagnosis (cadx)," in *Iberoamerican Congress on Pattern Recognition*. Springer, 2013, pp. 326–333.
- [23] R. Khaled, M. Helal, O. Alfarghaly, O. Mokhtar, A. Elkorany, H. El Kasas, and A. Fahmy, "Categorized contrast enhanced mammography dataset for diagnostic and artificial intelligence research," *Scientific Data*, vol. 9, no. 1, p. 122, 2022.
- [24] F. Strand, "CSAW-CC (mammography)," 2022. [Online]. Available: <https://doi.org/10.5878/45vm-t798>
- [25] N. Wu, J. Phang, J. Park, Y. Shen, Z. Huang, M. Zorin, S. Jastrzebski, T. Fevry, J. Katsnelson, E. Kim *et al.*, "Deep neural networks improve radiologists' performance in breast cancer screening," *IEEE transactions on medical imaging*, vol. 39, no. 4, pp. 1184–1194, 2019.